Effect of Channel Size on Liquid-Liquid Plug Flow in Small Channels

Dimitrios Tsaoulidis and Panagiota Angeli
Dept. of Chemical Engineering, University College London, Torrington Place, London WC1E 7JE, U.K.

DOI 10.1002/aic.15026
Published online September 22, 2015 in Wiley Online Library (wileyonlinelibrary.com)

The hydrodynamic properties of plug flow were investigated in small channels with 0.5-, 1-, and 2-mm internal diameter, for an ionic liquid/aqueous two-phase system with the aqueous phase forming the dispersed plugs. Bright field Particle Image Velocimetry combined with high-speed imaging were used to obtain plug length, velocity, and film thickness, and to acquire velocity profiles within the plugs. Plug length decreased with mixture velocity, while for constant mixture velocity it increased with channel size. Plug velocity increased with increasing mixture velocity and channel size. The film thickness was predicted reasonably well for $\mathrm{Ca} > 0.08$ *by Taylor's (Taylor, J Fluid Mech. 1961;10(2):161–165) model. A fully developed laminar profile was established in the central region of the plugs. Circulation times in the plugs decreased with increasing channel size. Pressure drop was predicted reasonably well by a modified literature model, using a new correlation for the film thickness derived from experimental values.* © 2015 The Authors AIChE Journal published by Wiley Periodicals, Inc. on behalf of American Institute of Chemical Engineers *AIChE J*, 62: 315–324, 2016
Keywords: hydrodynamics, scale-up, liquid-liquid, ionic liquid, μ-PIV

Introduction

Two-phase flows (gas-liquid, liquid-liquid) in small channels have found numerous applications in, among others, (bio)chemical analysis and synthesis, fuel cells, thermal management systems, separation processes (e.g., solvent extraction), emulsification, and polymerization, driven by demands on sustainable and efficient continuous processing.[1,2] Small scale devices allow fast mixing and enhanced mass transfer because of features such as thin fluidic films, high specific interfacial areas, recirculation within phases, and convection induced by surface tension gradients.[3]

A common configuration during the flow of two immiscible liquids in small channels is the plug (slug or segmented) pattern where one phase forms elongated drops (plugs) with size larger than the channel size, separated by continuous phase slugs. Mass transfer is enhanced by the presence of the continuous phase film that separates the plugs from the channel wall and the internal circulation within each phase. The convective circulation currents help to renew the interfaces and enhance diffusive mass transport. From the various configurations that have been used to generate plug flow (e.g., flow focusing, Y- or T-junction inlets), the T-shaped one is very common.[4] Plug formation in small channels is mainly affected by the interfacial and shear forces, that dominate the flow. Depending on the values of the *Ca* number, either one or both forces can be significant as the dispersed plug forms and obstructs the continuous phase while the pressure that builds behind it pushes the plug away from the inlet until it breaks.[5–9] For the prediction of the plug size different factors, such as volumetric flow rates and ratios of the two phases and widths of the main and side channels, have been considered in scaling law models and semiempirical correlations. In these models, the plug size is independent of the *Ca* number.[5,10,11] However, findings suggest that, parameters such as surface wettability, channel depth, and fluid properties also affect the plug size.[12–16] Internal circulation in the continuous and the dispersed phases is key parameter for enhancing mass transfer in plug flow. In aqueous-organic and organic-ionic liquid two-phase flows, it has been found that vortices in the continuous phase occupy almost the whole length of the segment, while the circulation within the dispersed plugs is affected by the phase properties, the film thickness and the tapered shape of the plug.[17,18] The parameters that are used to quantify mixing are the ratio of the vortex to the plug/slug length, and the nondimensional circulation time, τ, which relates the vortex circulation time, $t_{\mathrm{circ}} = \frac{V_{\mathrm{circ}}}{Q_{\mathrm{circ}}}$ (the average time to displace material from one side of the plug to the other) to the time that a plug needs to travel a distance equal to its own length, $t_{\mathrm{travel}} = \frac{L_{\mathrm{p}}}{u_{\mathrm{p}}}$.[19,20] The vortex structure depends on the superficial velocities and in the case of the dispersed phase also on the film thickness separating the plug from the wall and its shape. For a better understanding of the vortex circulation characteristics, a detailed knowledge of the velocity profiles in the phases is required. Micro-Particle Image Velocimetry (μ-PIV) has been used to obtain velocity fields in gas-liquid[20–22] and liquid-liquid[18,19,23,24] small channel flows.

Correspondence concerning this article should be addressed to P. Angeli at p.angeli@ucl.ac.uk

Table 1. Correlations for the Normalized (Against Channel Radius) Film Thickness (δ/R) for Gas-Liquid Taylor Flow

Dimensionless Film Thickness	Range of *Ca* Number	Reference
$\frac{\delta}{R} = 0.5\sqrt{Ca}$	$7.5{\cdot}10^{-5} < Ca < 0.01$	1,25
$\frac{\delta}{R} = 1.34Ca^{2/3}$	$Ca < 0.003$	26
$\frac{\delta}{R} = 0.36\left(1 - \exp\left(-3.1Ca^{0.54}\right)\right)$	$9.5{\cdot}10^{-4} < Ca < 1.9$	27
$\frac{\delta}{R} = \frac{1.34Ca^{2/3}}{1+2.5(1.34Ca^{2/3})}$	$10^{-3} < Ca < 1.4$	28

An important parameter in plug flow is the thickness of the film, which surrounds the dispersed plugs and depends on fluid properties, average velocity, flow rate ratio, and channel material and size. In Table 1, the most referenced models on film thickness in gas-liquid systems are presented.[2] There is a large number of investigations on film thickness originating from the experimental work by Taylor[29] and the theoretical analysis by Bretherton[26] at low *Ca* numbers (<0.003). Bretherton,[26] assuming inviscid flow, found that the film thickness was proportional to $Ca^{2/3}$. Aussillous and Quéré[28] identified two different regimes for plug flow, that is, the visco-capillary and the visco-inertia. In the visco-capillary regime, film thickness depends only on *Ca* number, and the data agreed well with Taylor's[29] results and Bretherton's[26] model. In the visco-inertia regime at higher *Ca* ($Ca > 10^{-3}$) their results deviated from Taylor's findings, as inertia becomes important, and the film thickness increases. Han and Shikazono[30] in gas-liquid horizontal flows in circular channels with 0.3 to 1.3 mm internal diameter found that the film thickness varied along the bubble because of gravity as the *Bo* number increased. They proposed an empirical correlation based on *Ca*, *Re*, and *We* numbers. At low *Ca* numbers the film thickness was found to be a function of only *Ca*, as the effect of the inertial forces is negligible. However, inertia effects cannot be neglected at higher *Ca* numbers, where with increasing *Re* the film thickness initially reduces and then increases again. In a similar study in millimeter-sized channels ($d = 1.12$, 1.69, and 2.12 mm), Leung et al.[31] found that by increasing the channel diameter the shape of the bubble loses its symmetry. Mac Giolla Eain et al.[32] reported that the film thickness in horizontal liquid-liquid flows was affected by the plug length and the continuous phase properties. Existing models could not predict their experimental results and a new model based on *Ca* and *We* numbers was proposed.

The geometric characteristics of plug flow such as plug length and film thickness affect pressure drop and are taken into account in predictive models. Pressure drop models usually interpret this pattern as a series of unit cells consisting of one plug and one slug, and consider frictional contributions from the two phases and the film, and interfacial contributions from the front and rear cups of the plug.[4,13,33,34]

In this article, a liquid-liquid system of TBP/$[C_4mim][NTf_2]$ (ionic liquid phase, see Figure 1) and HNO_3 aqueous solution (aqueous phase) is studied. The investigations are complementary to current research on intensified extraction separations relevant to spent nuclear fuel reprocessing using small scale extraction units.[35–37] Ionic liquids have been suggested as efficient and green alternatives to common solvents because of high-partition coefficients and negligible volatility and flammability at common industrial conditions.[38] Compared to common organic solvents, ionic liquids are more viscous and dense than aqueous solutions and have lower interfacial tension than aqueous-organic systems, which would affect the hydrodynamic behavior in two-phase flows.[34] Despite their superior performance, extensive use of ionic liquids is prevented by high production costs.[39] Extractions in small channels, where the amount of solvent required is less, would abate the problem of the high cost. There are very few studies on the flow behavior of ionic liquid two-phase systems in small channels and none that addresses effects of channel size. In this work, the hydrodynamic features (plug length and velocity, and film thickness), the mixing characteristics (circulation time and vortex structure), and the pressure drop of the two-phase system are studied in channels with dimensions from micrometer to millimeter (0.5–2 mm internal diameter) over *Ca* numbers that range from 0.03 to 0.18. A nonconventional bright field Particle Image Velocimetry (PIV) system combined with high-speed imaging was used to study flow characteristics. This approach avoids the use of lasers and complicated optics while it offers increased time resolution that is challenging in fluorescence microscopy.

Materials, Experimental Setup and Procedure

Materials

The two immiscible phases used in this work were a tributylphosphate (TBP)/ionic liquid mixture (30% v/v) and a HNO_3 solution (3 M). The ionic liquid is $[C_4mim][NTf_2]$ (viscosity $\mu = 0.052$ Pa s and density $\rho = 1420$ kg m^{-3}) and was prepared at the QUILL research centre, Queen's University of Belfast. The TBP was obtained from Sigma-Aldrich. The HNO_3 aqueous solution of 3 M was prepared in the UCL laboratory from general purpose HNO_3 (65%) solution by Fisher Scientific. The interfacial tension of the two-phase system ($\gamma = 10.01$ mN m^{-1}) was measured in the UCL laboratory with a Kruss DSA 100 drop analyzer system based on the pendant drop method. The TBP/ionic liquid mixture was preequilibrated with an aqueous solution of 3 M nitric acid in a flask by shaking vigorously for 20 min. This was necessary as the ionic liquid absorbs some amount of water (hygroscopic). For the flow experiments, the TBP/ionic liquid phase was separated and brought into contact with fresh nitric acid solution (3 M) which was seeded with 3.2 μm polymer microspheres (0.5–1% v/v, depending on the flow rates and the channel diameter). The viscosity of the saturated TBP/IL mixture, measured with a digital rheometer DV-III Ultra (Brookfield), was 0.029 Pa s.

Experimental setup

The experimental setup used for the two-phase flow investigations is depicted in Figure 2. High-precision pumps (Kd Scientific) were used to feed separately the two phases into the test section. The mixing zone was a T-junction made of Teflon with all the branches having the same internal diameter (*d*) as

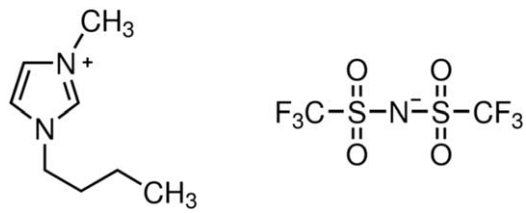

Figure 1. Chemical structure of the ionic liquid 1-butyl-3-methylimidazolium bis{(trifluoromethyl)sulfonyl}amide $[C_4mim][NTf_2]$.

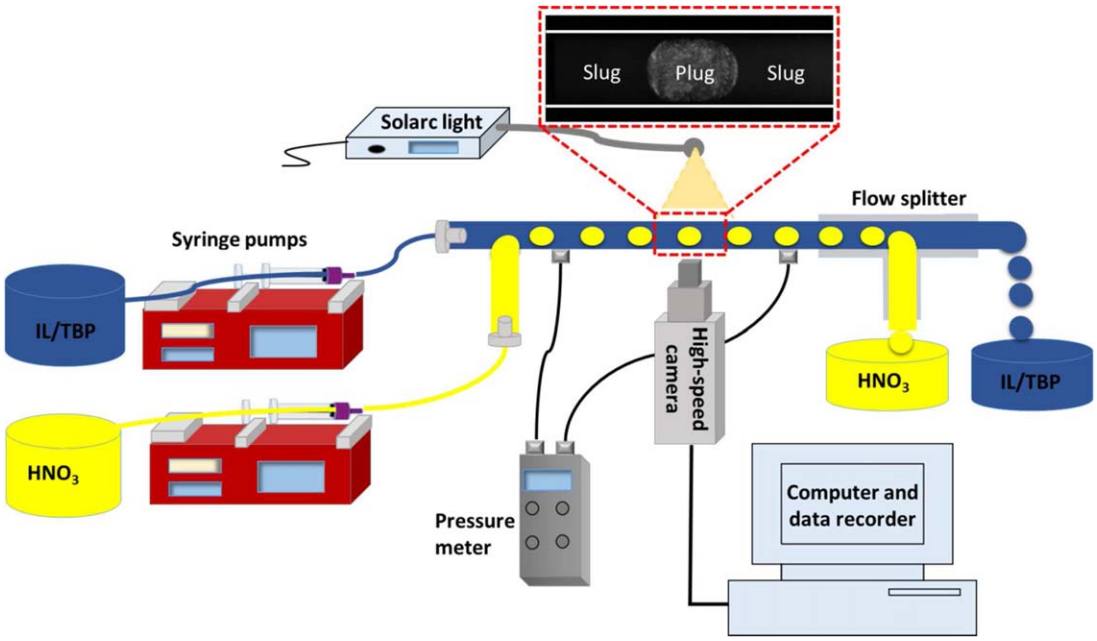

Figure 2. Schematic of the experimental setup.

[Color figure can be viewed in the online issue, which is available at wileyonlinelibrary.com.]

that of the main test channel. From the T-junction, the fluids entered into the test channel, also made of Teflon, which could have three different internal diameters, 0.5, 1, and 2 mm.

The total volumetric flow rate (Q_{mix}) varied from 7 to 340 $cm^3\ h^{-1}$, while the ratio of the two phases Q_{IL}/Q_{aq} varied from 0.5 to 1. Plug flow was established in all cases with the aqueous phase flowing as noncontinuous plugs within the TBP/ionic liquid phase (carrier phase). Pressure drop along the channels was measured with a digital differential pressure meter Comark C9555 (accuracy $\pm 0.2\%$), which was connected to two pressure ports 10 cm apart, as shown in Figure 2. The temperature was monitored during the experiments and remained constant.

Measurement of velocity fields and image processing

A bright field (shadowgraphy) Micro-Particle Image Velocimetry (μ-PIV) system was used to measure the velocity fields inside the aqueous plugs and to study the hydrodynamic properties of the two-phase system such as plug size and film thickness. The aqueous phase, which contained the polymer microspheres and the channel, were backlit with a 60 Watt continuous white arc lamp, which offers an even illumination of the flow field. In the acquired images, particles appeared dark on a bright background. A CMOS high-speed camera (Photron Fastcam-ultima APX) with a maximum resolution of 1024 $\times$ 1024 pixels, equipped with a magnification lens (LEICA Monozoom 7 optical system), acquired 2MP 10-bit images continuously at 2000–8000 Hz (depending on the total flow rate). The field of view was determined by the objective lenses of the camera (extending lenses: 0.75×, 0.5×, 0.25×, and shortening lenses: 1.5×, 2×) depending on the length of the aqueous plug, while the pixel size varied from 2.58 to 5.75 μm. Both the camera and the channel were placed at micrometer stages and traverses, which allowed a 3-D relative motion between them so as to focus precisely on the desired observation plane, approximately located at the channel midplane. The precision traverse was calibrated using the front wall of the channel as a reference. The capillary was enclosed in a flat visualization box filled with water to minimize reflections at the interface. The presence of the water in the visualization box and the short residence times ensured that the temperature of the fluids did not change during the experiments.

The commercial TSI PIV platform Insight 4G was used to calculate the displacement of the particles between windows across image pairs via a cross-correlation routine. The time interval between an image pair was chosen depending on the expected velocity inside the channel and the required spatial resolution. In the current study, a square discretization domain of 32 $\times$ 32 pixels with 50% overlap to satisfy the Nyquist sampling criterion was used.[40] A velocity spatial resolution from 16 to 46 μm was achieved along the x and y-axes, while the effective depth of field varied between 30 and 100 μm (as calculated from the characteristics of the optical system) following the calculations by Inoué and Spring.[41] The 2-D velocity field (u_x and u_y) was reconstructed within the Eulerian grid in which the domain was discretized, using the spatial calibration and the time interval between the correlation frames.

The system was validated by performing single aqueous phase experiments and comparing velocity profiles with the analytical solutions for laminar flow in circular channels. To maximize the signal-to-noise ratio, background subtraction was carried out prior to image cross-correlation. All the vector fields in the aqueous phase were validated by their signal-to noise-ratio and the spurious vectors found close to the interface were replaced using a median test in local 3 $\times$ 3 pixels neighborhoods. The distance from the interface that can be resolved varied between 30 and 80 μm for the different channels investigated. The circulation patterns were plotted using the Tecplot software embedded in Insight 4G. For the calculation of the film thickness (δ) and the plug size, a postprocessing routine was developed to detect the plug interface. The pixel intensity in the seeded plug was more uniform and intense, enabling image binarization using a threshold pixel value to discriminate the aqueous medium from the TBP/IL phase. The channel wall location was identified by the same routine, using, however, a lower threshold value. The two

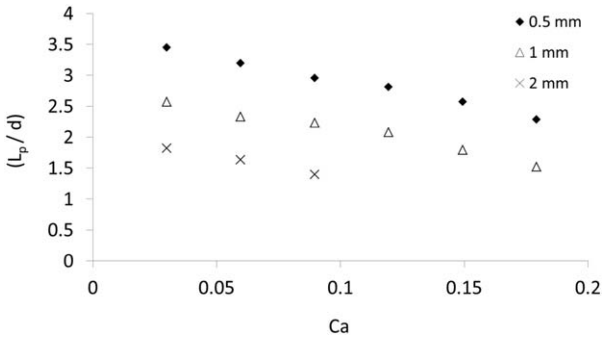

Figure 3. Normalized aqueous phase plug length, L_p/d against *Ca* number at three different channel sizes.

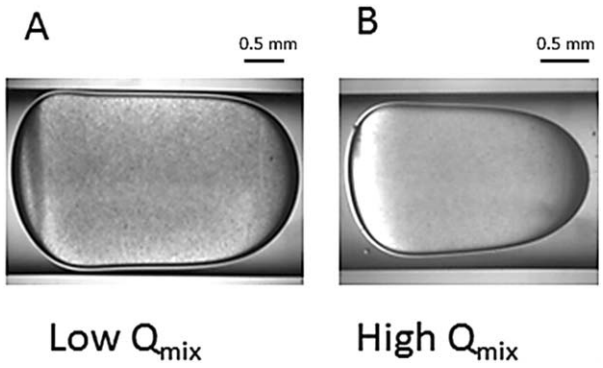

Figure 5. Plug shape at (A) low and (B) high total volumetric flow rate in the 2 mm channel.

binary masks for the channel and the aqueous phase were combined via image multiplication and the position and the size of the plug, and the film thickness were calculated. The values were averaged over a set of 30–60 images. It was found that at each set of flow conditions very regular plug lengths were established, as indicated by the low values of standard deviation (<3%).

Results and Discussion

Plug length

The plug length was measured from the high resolution images according to the procedure outlined in the previous section. At the experimental conditions of this work, plug formation is expected to be affected by both interfacial and shear forces as the *Ca* numbers are above the critical value of 10^{-2}.[8] At low *Ca* numbers, the emerging plug (HNO_3/aq) enters the main channel and grows until it blocks almost entirely its cross-section. The pressure in the continuous phase (TBP/IL) builds behind the forming plug and pushes it away from the inlet. As the *Ca* increases the shear of the continuous phase surrounding the forming plug also contributes to the plug breakage.

As can be seen in Figure 3, the normalized plug length L_p/d decreases as the mixture velocity and *Ca* number increase in all channels at equal phase flow rates. It was also found that for constant *Ca* number longer plugs are obtained as the channel size increases. The effect of the ionic liquid to aqueous phase flow rate ratio at constant mixture velocity is shown in Figure 4. In all channels sizes, the length of the aqueous plug

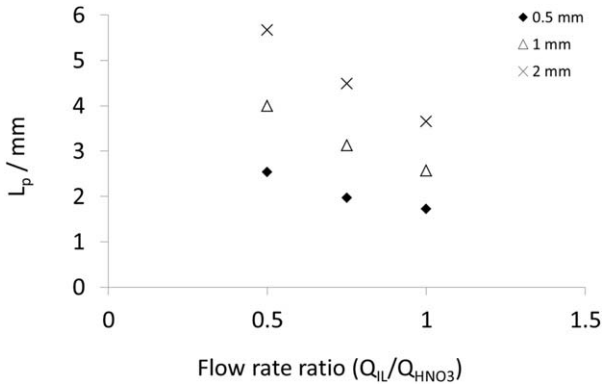

Figure 4. Plug length L_p against flow rate ratio (Q_{IL}/Q_{HNO3}) at constant mixture velocity u_{mix} = 0.01 m s^{-1}.

was found to decrease as the ratio increased. It can also be seen that the plug length increases with increasing channel diameter. This finding has an important impact on the design of a small-scale devices, as plug length for constant flow rates is related to the number of plugs and thus to interfacial area available for mass transfer.

The shape of the plug was also found to be affected by the total mixture velocity. By increasing the total volumetric flow rate the plugs acquired a "bullet" shape, where the rear interface became more flat, and the front more curved (Figure 5), which is in agreement with previous literature results.[26,30,42] As the *Ca* number increases the interfacial forces cannot sustain, the hemispherical shape of the front and the rear parts of the plugs.

Most models on plug length have been developed mainly for gas-liquid systems and are valid for low *Ca* numbers (<0.01).[5,10] In the current work, however, where ionic liquid is the continuous phase, the *Ca* numbers are large (0.03–0.18) and the suggested models were not able to predict plug lengths satisfactorily. Laborie et al.[15] studied experimentally gas-liquid Taylor flow in capillaries with internal diameter varying from 1 to 4 mm, and $55 < Re_{ub} = \rho d u_b/\mu < 2000$, $0.13 < Bo < 5$, $0.0015 < Ca < 0.1$ and found that the bubble length decreased when the capillary size increased, which is in contrast to the current work. Qian and Lawal[14] carried out numerical simulations in channels with widths varying from 0.25 to 3 mm for $0.000278 < Ca < 0.01$ and $15 < Re_{ub} < 1500$ and found that channel size and gas and liquid superficial velocities affected the length of the bubble, while surface tension and liquid viscosity had negligible effects. This model overpredicted the current experimental results with a mean relative error of 41%.

For liquid-liquid flows in particular, investigations of plug length are limited to low capillary numbers and channels of sub-mm size which do not cover the range of conditions used in the present work.[5,43,44] A correlation was developed from the current data in all channel sizes and mixture velocities from 0.01 to 0.06 m s^{-1}, which is given below

$$\frac{L_p}{d} = 2.2882 \cdot Ca_{mix}^{0.2728} \cdot Re_{mix}^{0.4617} \cdot Re_c^{-0.9634} \quad (1)$$

The dimensionless numbers were calculated as follows:

$$Ca_{mix} = \frac{\mu_c u_{mix}}{\gamma} \quad Re_{mix} = \frac{\rho_c d u_{mix}}{\mu_c}, \quad Re_c = \frac{\rho_c d u_c}{\mu_c},$$

where the subscripts c and mix are used for continuous and mixture, respectively, u is the superficial velocity, ρ is density, μ is viscosity, and γ is the interfacial tension. In the above

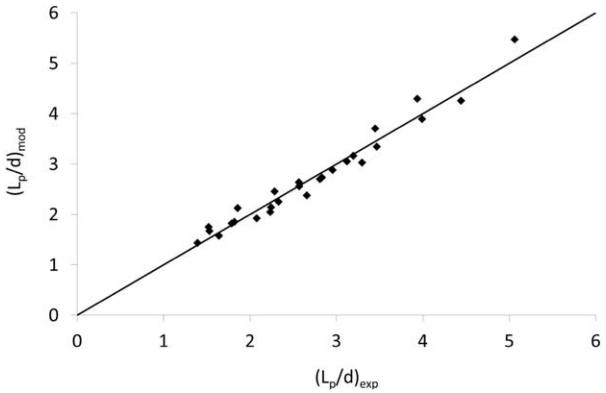

Figure 6. Comparison between experimental results and predictions of Eq. 1.

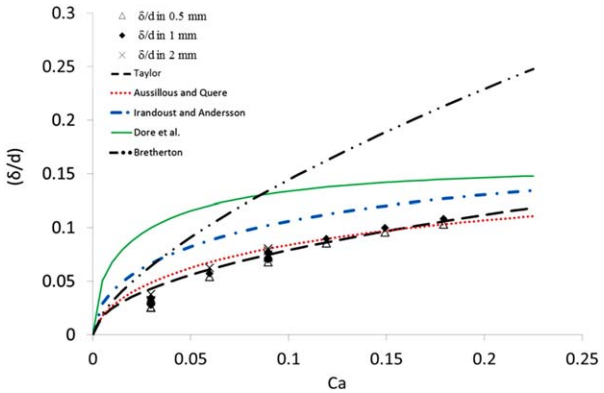

Figure 8. Nondimensional film thickness (δ/d) against *Ca* number for all experimental conditions and comparison with literature models.

[Color figure can be viewed in the online issue, which is available at wileyonlinelibrary.com.]

correlation, the viscosity ratio μ_d/μ_c was not included as it is $>1/29$ and does not affect the plug size for $Ca<0.1$.[16,45] The correlation predicted the experimental data with an average error of 6.7%. (Figure 6).

Film thickness

A thin film of the continuous ionic liquid phase was always present on the channel wall at the experimental conditions used. The thickness of the film was measured from the bright field PIV images by subtracting the width of the plug from the width of the channel and dividing by 2. The film thickness was measured at different positions along the region where the front and rear cups of the plug end and an average value was taken. For long plugs (low flow rates), a distinct flat film region between the rear and the front cups exists, while at higher flow rates, when the plugs exhibited a bullet shape, there was no apparent flat film region along the plug as can be seen in Figure 7. The standard deviation of the measurements of the film thickness was 3%.

The *Bo* numbers were less than 1 in the 0.5 and 1 mm channels (*Bo* equal to 0.07 and 0.27, respectively), which means that gravitational forces are not affecting the flow. The flow was axisymmetric in the 0.5 mm channel, while in the 1-mm channel the difference between the upper and lower film thickness was less than 5%. However, in the 2-mm channel, *Bo* was 1.12, which means that gravity can affect the flow, and the film thickness at the top was slightly different to that at the bottom of the channel. Similar findings of nonuniform film thickness along the dispersed phase plug were reported by

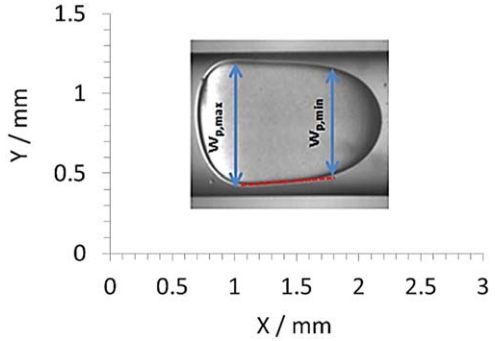

Figure 7. Image of a "bullet shape" plug with no apparent flat film region.

[Color figure can be viewed in the online issue, which is available at wileyonlinelibrary.com.]

Leung et al.[31] for a gas-liquid system in channel sizes with internal diameter larger than 1 mm.

As can be seen from Figure 8, the film thickness values agreed well with the model proposed by Taylor[29] for $Ca>0.08$, while a deviation from the model was found at low *Ca* numbers where the film thickness is small (13% average error). At $Ca>0.1$ the results agreed also with the model by Aussillous and Quere,[46] while for $Ca<0.1$ this model overpredicted the data (17% average error). The model by Bretherton[26] did not predict the experimental results for any of the channels tested, as the *Ca* numbers in the current work exceeded the range of applicability of the model ($Ca<0.003$). It is worth noting here that there are no correlations for film thickness in the literature for the fluidic system used in this study. The few available models for film thickness in liquid-liquid plug flows[32,47] under-predicted the current results. At high velocities inertial forces become important and affect the film thickness together with viscous and capillary forces. Mac Giolla Eain[32] proposed a model based on *Ca* and *We* numbers for a circular tube of 1.59 mm internal diameter, which however underestimated the present results by an average error of 20%. Analysis of the experimental results showed that the film thickness is dependent on *Ca* and *Re* numbers. A correlation (Eq. 2) was developed, which predicts the experimental results in all three channels with an average error of 7.5%.

$$\frac{\delta}{d}=0.329Ca_{\mathrm{mix}}^{0.6409}Re_{\mathrm{mix}}^{0.1067} \tag{2}$$

Plug velocity

The velocity of the plugs is important for mass-transfer applications as it is related to residence time in the microchannel unit. In Taylor flow, the film between the plug and the channel wall is expected to increase the plug velocity compared to the continuous phase velocity. At high *Ca* numbers when the film is thick, plug speed is also increased.

Under all conditions studied, a thin film was always present between the dispersed plug and the channel wall, which led to a plug velocity (u_p) always higher than the mixture velocity. In addition, as the mixture velocity increased, the difference between plug velocity and mixture velocity increased. As can be seen in Figure 9 at constant u_{mix} the plug was flowing faster as the channel diameter increased. The effect of channel size

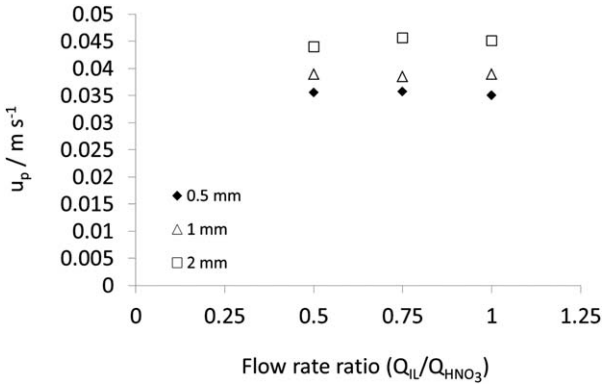

Figure 9. Plug velocity against flow rate ratio Q_{IL}/Q_{HNO3} in the different channels sizes at constant mixture velocity of 0.03 m s^{-1}.

is attributed to the difference in dimensionless film thickness, which for mixture velocity 0.03 m s^{-1} is almost 2% between 0.5 and 1 mm channels, and approximately 10% higher in the 2-mm channel. Plug velocity was found to be independent of the flow rate ratio (Figure 9) which means that the residence time of the plug in the channel is the same, even though the length of the plug changes.

The experimental plug velocity data are compared in Figure 10 with the empirical models from gas-liquid Taylor flow and the analytical approach of Bretherton.[26]

The results from all channel sizes agree reasonably well with Bretherton's model at low *Ca* numbers. At higher *Ca* numbers, the model overpredicted the data by more than 50%. The correlation proposed by Liu et al.,[48] based on experimental data in both circular and square capillaries, showed good agreement with the current findings with mean relative error of 11%.

Mixing characteristics

The velocity fields within the aqueous plugs are shown in Figure 11 for channel sizes 0.5 and 1 mm. It can be seen that the horizontal velocity component u_x dominates in both cases. The velocity reaches a maximum at the channel core and decreases toward the liquid-liquid interface. The velocity gradients are smaller in the large channel where a thicker film separates the plug from the wall. The bulk convective flow can clearly be seen in both cases.

For $L_p/d > 1$, a laminar profile is established at the center of the plugs which is shown with a dotted rectangle in Figure 11. The area of fully developed laminar flow depended on channel

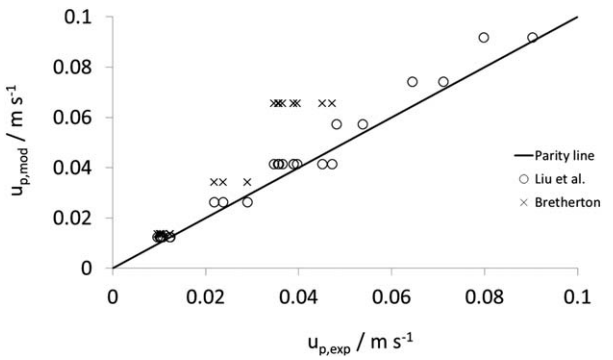

Figure 10. Comparison of the experimental plug velocity, u_p, with literature models.

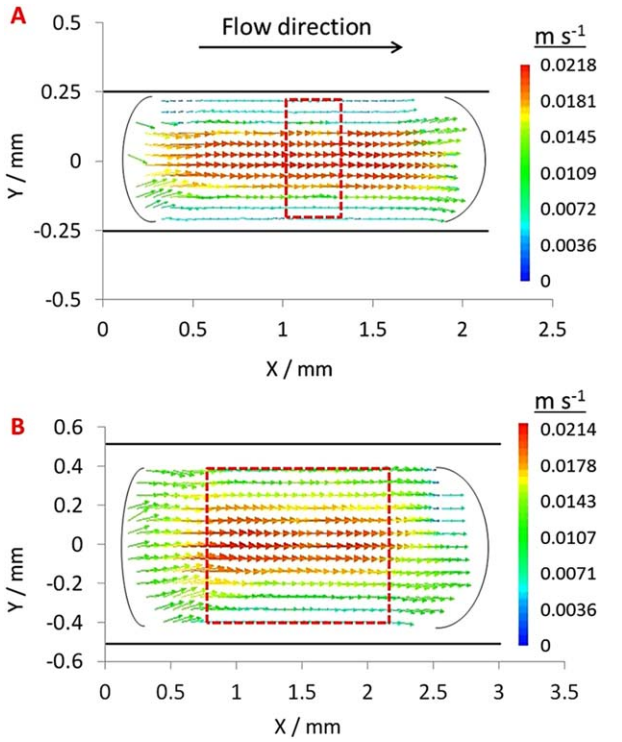

Figure 11. Ensemble average velocity field within an aqueous plug at $u_{mix} = 0.01$ m s^{-1} (flow rate ratio equal to 1) in a channel of (A) 0.5 mm internal diameter, and (B) 1 mm internal diameter.

For the profiles, 30 instantaneous velocity fields were averaged. [Color figure can be viewed in the online issue, which is available at wileyonlinelibrary.com.]

size and occupied approximately 45% of the plug length in the 0.5-mm channel (Figure 11A) while it increased to approximately 54% of the plug length in the 1-mm channel (Figure 11B). Two indicative velocity fields for the areas indicated in Figure 11 are shown in Figure 12, where the data agree well with the laminar profile within 6% mean relative error for both channels. The highest error was found at locations close to the interface.

Average profiles of the horizontal velocity component u_x normalized against the maximum velocity in the plug are shown in Figures 13 and 14 for the 1 mm channel size. The profiles were averaged over the area of fully developed laminar flow. In Figure 13, the velocity profiles of a 2.6 mm long plug at two different mixture velocities show that the velocity profiles are symmetrical about the channel axis.

The velocity profiles for a constant mixture velocity ($u_{mix} = 0.01$ m s^{-1}) are plotted in Figure 14 for two different plug lengths. The velocity profile within the longer plug had larger gradients compared to the shorter plug. These differences are attributed to differences in the thickness and uniformity of the film that surrounds the plugs that would affect the velocity profiles.

The circulating patterns within the aqueous plugs were calculated by subtracting the plug velocity from the averaged local velocity values (Figure 15). Two typical counter-rotating vortices, symmetrical to the channel centerline were found for most cases investigated. The symmetry indicates that there is no interaction between the upper and the lower halves of the plug, which results to a lower mixing efficiency. The

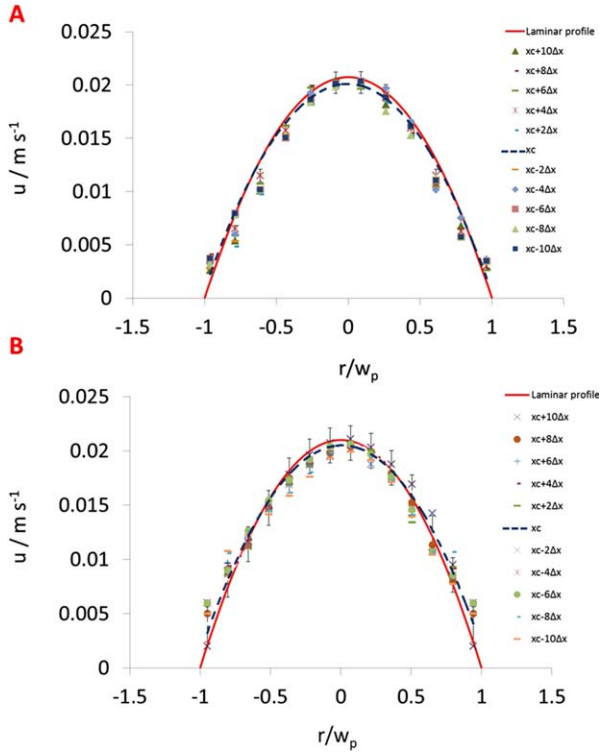

Figure 12. Profiles of the horizontal component of the total velocity across the aqueous plug at mixture velocity of 0.01 m s^{-1} (flow rate ratio equal to 1).

***xc* is the axial location of the plug centre while the spacing between profiles, Δx, is approximately equal to 0.041 and 0.068 mm in the 0.5 and 1 mm channels, respectively. [Color figure can be viewed in the online issue, which is available at wileyonlinelibrary.com.]**

circulation results in two stagnation points within the plugs. Their positions were determined by plotting the horizontal velocity components (u_x), averaged over the area of fully developed laminar flow (dotted areas in Figure 11), relative to the plug velocity against the plug width; the stagnation points are located at the intercept of the profile with the horizontal axis (Figure 16). In Figure 16, the effect of plug length (by changing the ionic liquid volume fraction) on the location of the stagnation points at constant mixture velocity ($u_{mix} = 0.01$ m s^{-1}) is shown for the 1-mm channel. As the plug length increases, the stagnation points approach the centerline of the channel up to plug length of 3.1 mm, above which the stagnation points do not shift further. In all cases, the positions of the stagnation points for the upper and lower half of the plug were fairly symmetric.

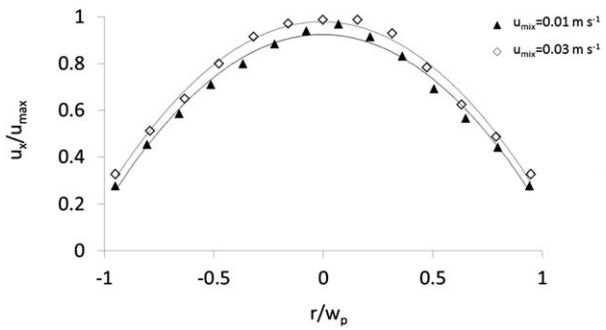

Figure 13. Velocity profiles of the horizontal velocity component u_x (normalized with the maximum velocity) for a plug with length 2.6 mm in the 1 mm channel.

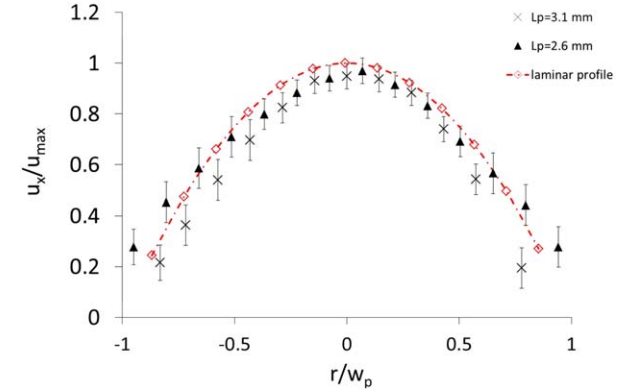

Figure 14. Velocity profiles of the horizontal velocity component u_x (normalized with the maximum velocity) at constant mixture velocity 0.01 m s^{-1} in the 1 mm channel.

[Color figure can be viewed in the online issue, which is available at wileyonlinelibrary.com.]

For a constant plug length, the position of the stagnation points seems to be only slightly affected by mixture velocity (u_{mix}) (Figure 17) and hence by the velocity ratio (u_p/u_{mix}) in the channel sizes studied. The location of the stagnation points found experimentally was compared against the equation proposed by Thulasidas et al.[20]

$$r^0 = \frac{R}{\sqrt{2}}\sqrt{2-\psi} \tag{3}$$

where r^0 is the radial position of the center of the toroidal vortex, R is the radius of the channel, and $\psi = u_p/u_{mix}$. To apply this equation to the stagnation points found in the dispersed phase, the plug half width is used instead of the channel radius.

In the case of constant mixture velocity (Figure 16), the location of the stagnation points was predicted with an error of 9% for the three plug lengths. The lowest error was observed in the case of the shortest plug of 2.6 mm (error of 1.7%). However, the equation did not predict as well the locations of the stagnation points when the mixture velocity increased for constant plug length.

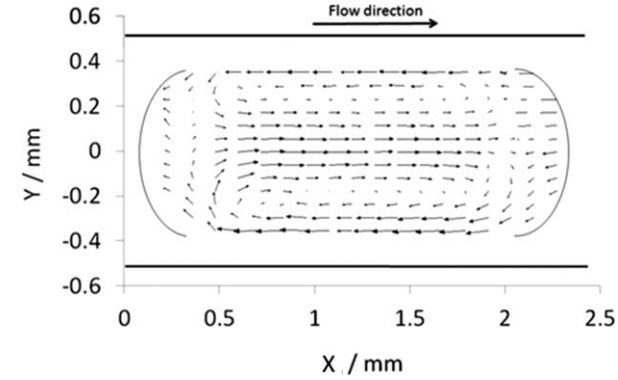

Figure 15. Internal circulation in the aqueous plug at mixture velocity of 0.01 m s^{-1} in the 1 mm channel.

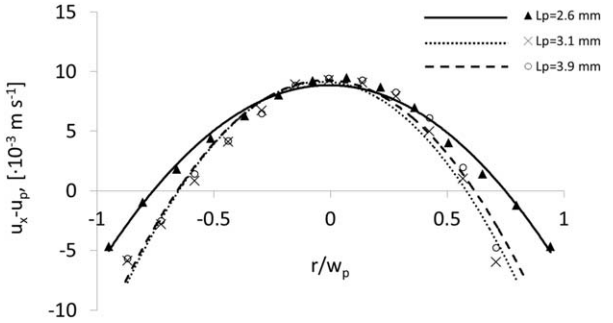

Figure 16. Horizontal velocity component, u_x, relative to the plug velocity, u_p, against the dimensionless plug radius for different pug lengths at mixture velocity of 0.01 m s^{-1} (Q_{mix} = 28.3 cm^3 h^{-1}).

The stagnation points are found from the intercepts of the lines with the horizontal axis.

Circulation within plugs, which improves internal mixing, can be quantified with the nondimensional circulation time, τ, which is calculated at a planar domain in the channel center as follows[19]:

$$\tau(x) = \frac{L_d\, y_0}{\int_0^{y_0} u(x,y)\, dy} \frac{u_p}{L_p} \cong \frac{u_p\, y_0}{\Delta y \sum_{i=1}^{i=N} u_i\big|_x} \tag{4}$$

The circulation time was calculated only for the region of the plug where the streamlines are closed (see for example Figure 15) and was averaged over 25–35 cross-correlated image pairs. For plugs of the same length, the nondimensional circulation time increases slightly with mixture velocity as can be seen in Figure 18, which indicates more intense mixing. In addition, τ is fairly constant across the length of the plug which means that the circulation patterns are regular.

For constant mixture velocity, the nondimensional circulation time was found to decrease with increasing plug length. With increasing channel size, for the same mixture velocity, the dimensionless circulation time decreases. In the 0.5 mm channel, τ has values in the range of 1.95–2.35, while in the 1 and 2 mm channels τ varies in the range of 3.41–3.95 and 4.20–4.75, respectively. This is in agreement with the increase in plug length with channel size (see Figure 4).

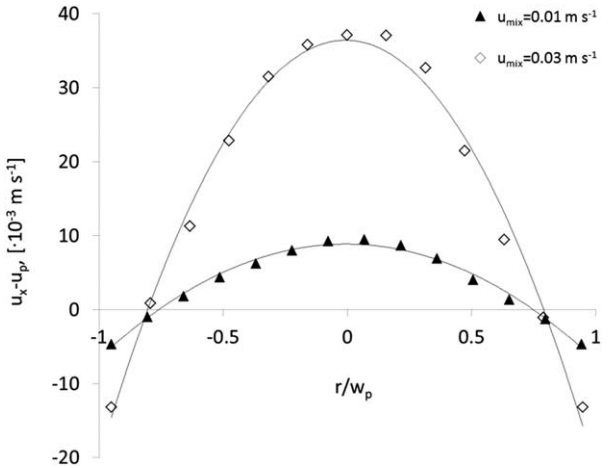

Figure 17. Horizontal velocity component u_x relative to the plug velocity, u_p, against the dimensionless plug radius for plug length L_p = 2.6 mm.

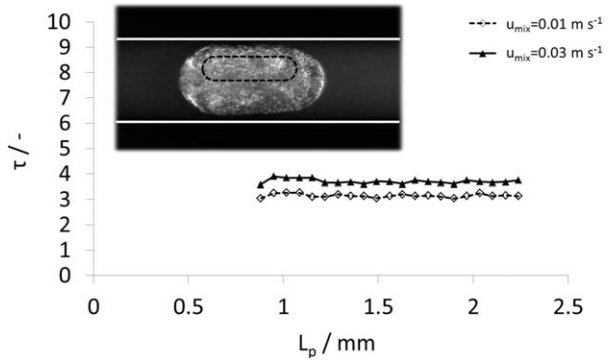

Figure 18. Nondimensional circulation time across the upper half of the plug at different mixture velocities u_{mix}, for plug length L_p = 2.6 mm in the 1 mm channel.

Dotted line represents the region of the plug where the streamlines are closed.

Pressure drop

Pressure drop was measured in all experimental cases over a length of 10 cm with a standard deviation of 4%. The results shown in Figure 19 indicate that pressure drop increases with increasing mixture velocity (at flow rate ratio equal to 1) and decreases with increasing channel size. Pressure drop was always higher than that of the single phase ionic liquid having the same flow rate as in the two-phase mixture.

Three terms are considered to contribute to the frictional pressure drop during plug flow, (1) frictional pressure drop of the continuous phase slug, (2) frictional pressure drop of the dispersed phase plug, and (3) the interfacial pressure drop at the front and rear caps of the plug; these contributions are summarized in the following equation (Eq. 5)3,[33,42]

$$\Delta P_{total} = \frac{8u_p \alpha L}{\frac{R^2-(R-\delta)^2}{\mu_c} + \frac{0.5(R-\delta)^2}{\mu_d}} + \frac{8u_{mix}\mu_c(1-\alpha)L}{R^2} + \frac{L}{l_u} C(3Ca)^{2/3} \frac{\gamma}{d} \tag{5}$$

In this equation, it is assumed that the film surrounding the plug is moving. The first two terms in Eq. 5 refer to the frictional pressure drop in the plug and the slug, respectively, and can be calculated from the Hagen–Poiseuille equation assuming fully developed laminar flow. In the first term, it is assumed that the film surrounding the plug is uniform across

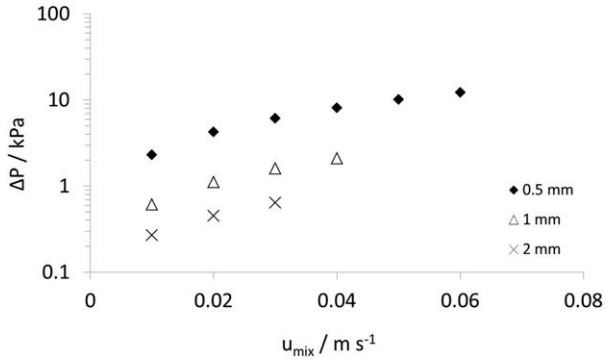

Figure 19. Experimental pressure drop during plug flow against mixture velocity for different channel sizes at flow rate ratio equal to 1.

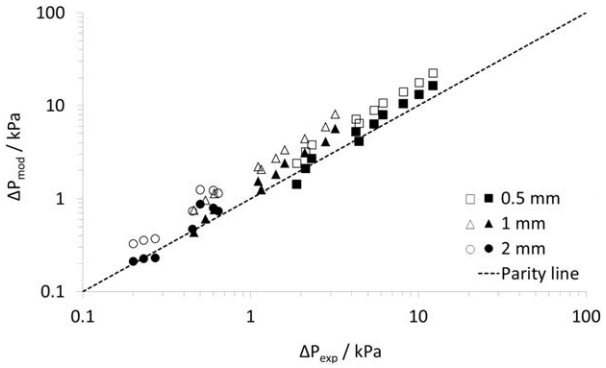

Figure 20. Comparison of the pressure drop calculated via the moving film model[33] to the experimental results of this work for three different channel sizes, mixture velocities from 0.01 to 0.06 m s^{-1}, and flow rate ratios (Q_{IL}/Q_{aq}) from 0.5 to 1.

Open symbols correspond to $C = 7.16$ and filled symbols to $C = 1.7$ in Eq. 5.

its length. However, as shown previously, the film thickness can vary along the plug depending on the operating conditions. The velocity u_p is the plug velocity. The velocity of the continuous phase in the second term is taken equal to the mixture velocity. The third term refers to the Laplace pressure at the front and the back interfaces of the plug as calculated by Bretherton[26] for low Ca numbers.

The estimation of the interfacial pressure is highly dependent on the interface curvature of the front and back caps of the plug as well as other factors such as Marangoni effects,[49] resulting in deviations from the Bretherton[26] theory; different values of the C parameter have thus been proposed in the literature. Jovanovic et al.[33] suggested C equal to 7.16 for the calculation of the interfacial pressure drop in circular channels of 248 and 498 μm internal diameters, where both the front and the back of the plugs are semispherical, assuming negligible gravitational, viscous and inertial forces compared to the interfacial forces. Gupta et al.[13] set C equal to 9.04 to account for the slight change in curvature between the front and back caps in a circular channel of 1.06 mm internal diameter. They found good agreement between predictions from Eq. 5 with computational fluid dynamics (CFD) simulations for sufficiently long plugs. Moreover, different values of C have been suggested for noncircular channels.[50,51]

The predictions of Eq. 5 were compared against the current experimental results from the three different channel sizes. Bretherton's[26] equation for film thickness is not valid for the high capillary numbers and the large film thicknesses (>1% of the channel radius) of the current study (see Figure 8); thus, the film thickness calculated from Eq. 2 was used instead. It was found that Eq. 5 overpredicted the experimental pressure drop data for the whole range of Ca numbers investigated for the two curvature parameters $C = 7.16$ and $C = 9.14$ with mean relative error of about 42% and 48%, respectively, for the three channel sizes used (Figure 20). This deviation is attributed to the nonuniform film thickness along the plug and the shape of the plug caps. At low flow rates the deformation of the front and back caps of the plug is not significant while at higher flow rates and channel sizes inertia and gravitational forces result in a bullet plug shape and nonuniform film thickness (see Figure 5). To account for the change of plug front and back curvature, the parameter C was modified. As shown in previous work,[33] the value of C decreases as the Ca and Re numbers increase. It was found that $C = 1.7$ improved the predictions over the range of Ca numbers investigated ($0.03 < Ca < 0.18$) with mean relative error of 14% (see Figure 20). Equation 5 with the modified curvature parameter ($C = 1.7$) was also found to predict well pressure drop data in a similar ionic liquid/water system[34] in a 0.22 mm channel for Ca numbers ranging from 0.07 to 0.55 with an average error of 6%.

Conclusions

The hydrodynamic characteristics of the plug flow pattern were investigated during liquid-liquid flows in small channels of different sizes. The two immiscible phases were an ionic liquid and an aqueous solution, with the aqueous phase forming the dispersed plugs under all conditions. High speed bright field PIV was used to obtain the geometric properties of the plugs and the velocity profiles within the aqueous phase. It was found that as the mixture velocity increased at equal flow rates of the two phases, the length of the plugs decreased because of the rapid penetration of one phase into the other while at constant mixture velocity the plug length increased with increasing channel diameter. Plug length was compared against literature models but little agreement was found. A correlation was developed based on dimensionless groups, which predicted reasonably well the plug lengths in all channel sizes studied. It was also found that in all channel sizes, the plug velocity (u_p) was higher than the mixture velocity, while at constant u_{mix} the plug velocity increased as the channel size increased.

Moreover, a thin film was found to surround the plugs at all experimental conditions. The film thickness was compared against literature models and good agreement was found with the model proposed by Taylor[29] for $Ca > 0.08$ (3% average error); the largest deviations occurred at low Ca numbers where the film thickness is small. A new correlation was proposed, which predicted the experimental results with 7.5% error.

For sufficiently long plugs ($L_p/d > 1$) a laminar profile was fully established away from the front and rear ends but the area it occupied depended on channel size. Two typical counter-rotating vortices were formed at the upper and lower half of the plug, symmetrical about the channel centerline. At constant mixture velocity, with increasing plug length the stagnation points moved closer to the channel centerline. However, for constant plug length the location of the stagnation points was independent of the mixture velocity. Circulation times within the plugs were found to increase with increasing channel size, which suggests less efficient mixing. It was also found that for the same channel diameter an increase in plug length at the same mixture velocity increased the circulation time. A pressure drop model, modified from a literature correlation, showed relatively good agreement with the experimental data for all channel sizes tested.

Acknowledgments

The authors would like to acknowledge Prof. Kenneth R. Seddon and Dr. Natalia V. Plechkova of Queen's University Ionic Liquids Laboratories (QUILL) for providing the ionic liquids. The authors would also like to thank the Engineering and Physical Science Research Council UK (EPSRC) for providing the Photron Fastcam-ultima APX high-speed camera for this work.

Literature Cited

1. Stankiewicz AI, Moulijn JA. Process intensification: transforming chemical engineering. *Chem Eng Prog*. 2000;96(1):22–34.
2. Angeli P, Gavriilidis A. Hydrodynamics of Taylor flow in small channels: a review. *Proc Inst Mech Eng C J Mec*. 2008;222(5):737–751.
3. Tung KY, Li CC, Yang JT. Mixing and hydrodynamic analysis of a droplet in a planar serpentine micromixer. *Microfluid Nanofluidics*. 2009;7(4):545–557.
4. Kashid MN, Agar DW. Hydrodynamics of liquid–liquid slug flow capillary microreactor: flow regimes, slug size and pressure drop. *Chem Eng J*. 2007;131(1):1–13.
5. Garstecki P, Fuerstman MJ, Stone HA, Whitesides GM. Formation of droplets and bubbles in a microfluidic T-junction-scaling and mechanism of break-up. *Lab Chip*. 2006;6(3):437–446.
6. van Steijn V, Kreutzer MT, Kleijn CR. μ-PIV study of the formation of segmented flow in microfluidic T-junctions. *Chem Eng Sci*. 2007;62(24):7505–7514.
7. Xu B, Cai W, Liu X, Zhang X. Mass transfer behavior of liquid–liquid slug flow in circular cross-section microchannel. *Chem Eng Res Des*. 2013;91(7):1203–1211.
8. De Menech M, Garstecki P, Jousse F, Stone H. Transition from squeezing to dripping in a microfluidic T-shaped junction. *J Fluid Mech*. 2008;595:141–161.
9. Thorsen T, Roberts RW, Arnold FH, Quake SR. Dynamic pattern formation in a vesicle-generating microfluidic device. *Phys Rev Lett*. 2001;86(18):4163–4166.
10. Leclerc A, Philippe R, Houzelot V, Schweich D, De Bellefon C. Gas–liquid Taylor flow in square micro-channels: new inlet geometries and interfacial area tuning. *Chem Eng J*. 2010;165(1):290–300.
11. van Steijn V, Kleijn CR, Kreutzer MT. Predictive model for the size of bubbles and droplets created in microfluidic T-junctions. *Lab Chip*. 2010;10(19):2513–2518.
12. Abadie T, Aubin J, Legendre D, Xuereb C. Hydrodynamics of gas–liquid Taylor flow in rectangular microchannels. *Microfluid Nanofluidics*. 2012;12(1–4):355–369.
13. Gupta R, Leung SS, Manica R, Fletcher DF, Haynes BS. Hydrodynamics of liquid–liquid Taylor flow in microchannels. *Chem Eng Sci*. 2013;92:180–189.
14. Qian D, Lawal A. Numerical study on gas and liquid slugs for Taylor flow in a T-junction microchannel. *Chem Eng Sci*. 2006;61(23):7609–7625.
15. Laborie S, Cabassud C, Durand-Bourlier L, Laine J. Characterisation of gas–liquid two-phase flow inside capillaries. *Chem Eng Sci*. 1999;54(23):5723–5735.
16. Christopher GF, Noharuddin NN, Taylor JA, Anna SL. Experimental observations of the squeezing-to-dripping transition in T-shaped microfluidic junctions. *Phys Rev E Stat Nonlin Soft Matter Phys*. 2008;78(3 Pt 2):036317.
17. Ufer A, Sudhoff D, Mescher A, Agar D. Suspension catalysis in a liquid–liquid capillary microreactor. *Chem Eng J*. 2011;167(2):468–474.
18. Scheiff F, Holbach A, Agar DW. Slug flow of ionic liquids in capillary microcontactors: fluid dynamic intensification for solvent extraction. *Chem Eng Technol*. 2013;36(6):975–984.
19. Dore V, Tsaoulidis D, Angeli P. Mixing patterns in water plugs during water/ionic liquid segmented flow in microchannels. *Chem Eng Sci*. 2012;80:334–341.
20. Thulasidas TC, Abraham MA, Cerro RL. Flow patterns in liquid slugs during bubble-train flow inside capillaries. *Chem Eng Sci*. 1997;52(17):2947–2962.
21. Malsch D, Kielpinski M, Merthan R, Albert J, Mayer G, Köhler JM, Süße H, Stahl M, Henkel T. μPIV-analysis of Taylor flow in micro channels. *Chem Eng J*. 2008;135:S166–S172.
22. Zaloha P, Kristal J, Jiricny V, Völkel N, Xuereb C, Aubin J. Characteristics of liquid slugs in gas–liquid Taylor flow in microchannels. *Chem Eng Sci*. 2012;68(1):640–649.
23. Kashid MN, Gerlach I, Goetz S, Franzke J, Acker JF, Platte F, Agar DW, Turek S. Internal circulation within the liquid slugs of a liquid-liquid slug-flow capillary microreactor. *Ind Eng Chem Res*. 2005;44(14):5003–5010.
24. King C, Walsh E, Grimes R. PIV measurements of flow within plugs in a microchannel. *Microfluid Nanofluidics*. 2007;3(4):463–472.
25. Fairbrother F, Stubbs AE. 119. Studies in electro-endosmosis. Part VI. The "bubble-tube" method of measurement. *J Chem Soc*.1935;1:527–529.
26. Bretherton FP. The motion of long bubbles in tubes. *J Fluid Mech*. 1961;10(2):166–188.
27. Irandoust S, Andersson B. Liquid film in Taylor flow through a capillary. *Ind Eng Chem Res*. 1989;28(11):1684–1688.
28. Aussillous P, Quéré D. Quick deposition of a fluid on the wall of a tube. *Phys Fluids (1994-present)*. 2000;12(10):2367–2371.
29. Taylor GI. Deposition of a viscous fluid on the wall of a tube. *J Fluid Mech*. 1961;10(2):161–165.
30. Han Y, Shikazono N. Measurement of the liquid film thickness in micro tube slug flow. *Int J Heat Fluid Flow*. 2009;30(5):842–853.
31. Leung SS, Gupta R, Fletcher DF, Haynes BS. Gravitational effect on Taylor flow in horizontal microchannels. *Chem Eng Sci*. 2012;69(1):553–564.
32. Mac Giolla Eain M, Egan V, Punch J. Film thickness measurements in liquid–liquid slug flow regimes. *Int J Heat Fluid Flow*. 2013;44:515–523.
33. Jovanović J, Zhou W, Rebrov EV, Nijhuis T, Hessel V, Schouten JC. Liquid–liquid slug flow: hydrodynamics and pressure drop. *Chem Eng Sci*. 2011;66(1):42–54.
34. Tsaoulidis D, Dore V, Angeli P, Plechkova NV, Seddon KR. Flow patterns and pressure drop of ionic liquid–water two-phase flows in microchannels. *Int J Multiphas Flow*. 2013;54:1–10.
35. Tsaoulidis D, Angeli P. Effect of channel size on mass transfer during liquid–liquid plug flow in small scale extractors. *Chem Eng J*. 2015;262:785–793.
36. Tsaoulidis D, Dore V, Angeli P, Plechkova NV, Seddon KR. Dioxouranium(VI) extraction in microchannels using ionic liquids. *Chem Eng J*. 2013;227:151–157.
37. Tsaoulidis D, Dore V, Angeli P, Plechkova NV, Seddon KR. Extraction of dioxouranium(VI) in small channels using ionic liquids. *Chem Eng Res Des*. 2013;91(4):681–687.
38. Plechkova NV, Seddon KR. Applications of ionic liquids in the chemical industry. *Chem Soc Rev*. 2008;37(1):123–150.
39. Birdwell JF Jr, McFarlane J, Hunt RD, Luo H, DePaoli DW, Schuh DL, Dai S. Separation of ionic liquid dispersions in centrifugal solvent extraction contactors. *Sep Sci Technol*. 2006;41(10):2205–2223.
40. Meinhart CD, Wereley ST, Santiago JG. PIV measurements of a microchannel flow. *Exp Fluids*. 1999;27(5):414–419.
41. Inoué S, Spring KR. *Video Microscopy: The Fundamentals (The Language of Science)*. New York: Plenum, 1997.
42. Kreutzer MT, Kapteijn F, Moulijn JA, Heiszwolf JJ. Multiphase monolith reactors: chemical reaction engineering of segmented flow in microchannels. *Chem Eng Sci*. 2005;60(22):5895–5916.
43. Xu J, Luo G, Li S, Chen G. Shear force induced monodisperse droplet formation in a microfluidic device by controlling wetting properties. *Lab Chip*. 2006;6(1):131–136.
44. Xu JH, Li SW, Tan J, Luo GS. Correlations of droplet formation in T-junction microfluidic devices: from squeezing to dripping. *Microfluid Nanofluidics*. 2008;5(6):711–717.
45. Liu H, Zhang Y. Droplet formation in a T-shaped microfluidic junction. *J Appl Phys*. 2009;106(3):034906.
46. Aussillous P, Quere D. Bubbles creeping in a viscous liquid along a slightly inclined plane. *Europhys Lett*. 2002;59(3):370–376.
47. Ghaini A, Kashid M, Agar D. Effective interfacial area for mass transfer in the liquid–liquid slug flow capillary microreactors. *Chem Eng Process: Process Intensif*. 2010;49(4):358–366.
48. Liu H, Vandu CO, Krishna R. Hydrodynamics of Taylor flow in vertical capillaries: flow regimes, bubble rise velocity, liquid slug length, and pressure drop. *Ind Eng Chem Res*. 2005;44(14):4884–4897.
49. Kreutzer MT, Kapteijn F, Moulijn JA, Kleijn CR, Heiszwolf JJ. Inertial and interfacial effects on pressure drop of Taylor flow in capillaries. *AIChE J*. 2005;51(9):2428–2440.
50. Wong H, Radke C, Morris S. The motion of long bubbles in polygonal capillaries. Part 2. Drag, fluid pressure and fluid flow. *J Fluid Mech*. 1995;292:95–110.
51. Van Steijn V, Kreutzer M, Kleijn C. Velocity fluctuations of segmented flow in microchannels. *Chem Eng J*. 2008;135:S159–S165.

Manuscript received Feb. 13, 2015, and revision received July 13, 2015.